Fully gapped superconductivity without sign reversal in the topological superconductor $PbTaSe_2$

Yue Sun,[1,2,*] Shunichiro Kittaka,[1,8] Toshiro Sakakibara,[1] Kazushige Machida,[3] R. Sankar,[4] Xiaofeng Xu,[5] Nan Zhou,[1,6] Xiangzhuo Xing,[6] Zhixiang Shi,[6] Sunseng Pyon,[7] and Tsuyoshi Tamegai[7]

[1]*Institute for Solid State Physics (ISSP), The University of Tokyo, Kashiwa, Chiba 277-8581, Japan*
[2]*Department of Physics and Mathematics, Aoyama Gakuin University, Sagamihara 252-5258, Japan*
[3]*Department of Physics, Ritsumeikan University, Kusatsu, Shiga 525-8577, Japan*
[4]*Institute of Physics, Academia Sinica, Nankang, Taipei 11529, Taiwan*
[5]*Department of Applied Physics, Zhejiang University of Technology, Hangzhou 310023, China*
[6]*School of Physics and Key Laboratory of MEMS of the Ministry of Education, Southeast University, Nanjing 211189, China*
[7]*Department of Applied Physics, The University of Tokyo, Bunkyo-ku, Tokyo 113-8656, Japan*
[8]*Department of Physics, Chuo University, Bunkyo-ku, Tokyo 112-8551, Japan*

(Received 9 April 2020; revised 7 July 2020; accepted 7 July 2020; published 21 July 2020)

We investigate the superconducting gap function of the topological superconductor $PbTaSe_2$. The temperature, magnetic field, and three-dimensional (3D) field-angle dependences of the specific heat prove that the superconductivity of $PbTaSe_2$ is fully gapped, with two isotropic *s*-wave gaps. The pair-breaking effect is probed by systematically increasing nonmagnetic disorders through H^+ irradiation. The superconducting transition temperature T_c is found to be robust against disorders, which suggests that the pairing should be sign preserved rather than sign reversed.

DOI: 10.1103/PhysRevB.102.024517

I. INTRODUCTION

Topological superconductivity (TSC) has stimulated great interests in condensed matter physics [1,2]. It is partly due to the possibility of hosting a Majorana bound state, which obeys the non-Abelian statistics, and can be used in topological quantum computation [3,4]. In real materials, the topological superconductors can be realized in two primary routes. One way is to make a heterostructure between conventional *s*-wave superconductors and topological insulators [5], quantum anomalous Hall insulators [6], or ferromagnetic atomic chains [7], where the proximity effect on a spin nondegenerate band induces TSC on the interface. Another way is to search materials naturally hosting TSC [1,8]. In the second route, both bulk TSC with spin-triplet *p*-wave pairing and surface TSC above a bulk spin-singlet *s*-wave superconductivity are realized [1,2,5,9–11]. In the second route, noncentrosymmetric superconductors are one of the most promising ways [12,13]. Due to the broken inversion symmetry, spin-orbit coupling becomes antisymmetric, which can lift spin degeneracy, and induce the topological state. It allows for the mixing of spin-singlet and spin-triplet pairing, suggesting both bulk and surface TSC are hopeful to be realized [14].

The noncentrosymmetric superconductor $PbTaSe_2$ shows a bulk superconducting transition temperature $T_c \sim 3.7$ K, with strong spin-orbit coupling, which results in a large Rashba splitting and the breaking of spin degeneracy [15]. Recent angle-resolved photoemission spectroscopy (ARPES) measurements reveal the existence of topological nodal lines near the Fermi surface, which are protected by reflection symmetry [16]. The topological state is also confirmed by the following scanning tunneling microscopy (STM) measurements [14], and a zero-energy bound state at the vortex core was also observed [14,17]. These results suggest that $PbTaSe_2$ is a promising candidate for TSC [14,16–21].

To reveal the origin and mechanism of the TSC in $PbTaSe_2$, it is crucial to probe its bulk gap function. Up to now, no breaking of time-reversal symmetry has been reported based on muon spin rotation and relaxation (μSR) experiments [22]. A fully gapped structure has been suggested by measurements of specific heat [23], thermal conductivity [24], penetration depth [25], and nuclear magnetic resonance (NMR) [26], while details about the gap structure such as whether it is multigap or single gap, isotropic or anisotropic, are still controversial [21,24,25]. In addition, most evidence for the fully gapped structure is obtained from excited quasiparticles (QPs) in the *ab* plane since the applied magnetic fields are along the *c* axis [23–25]. Hence, a *p*-wave-like gap structure with nodes along the k_z directions, which can host Majorana fermions in its side surface, has not been well identified [27–29]. Furthermore, even for a fully gapped structure, the pairing can be sign reversed or sign preserved. A well-known example is iron-based superconductors, where the gap function has no nodes but may still change sign between the electron and hole pockets [30,31]. To probe the gap structure including a possible sign reversal, a bulk technique capable of probing QP excitations with three-dimensional (3D) angle resolution, and a phase-sensitive probe are needed.

In this paper, we combined the measurements of 3D field angle-resolved specific heat (ARSH) and the disorder effects induced by H^+ irradiation to probe the gap function of $PbTaSe_2$. The former technique has a 3D angle resolution of

*sunyue@phys.aoyama.ac.jp

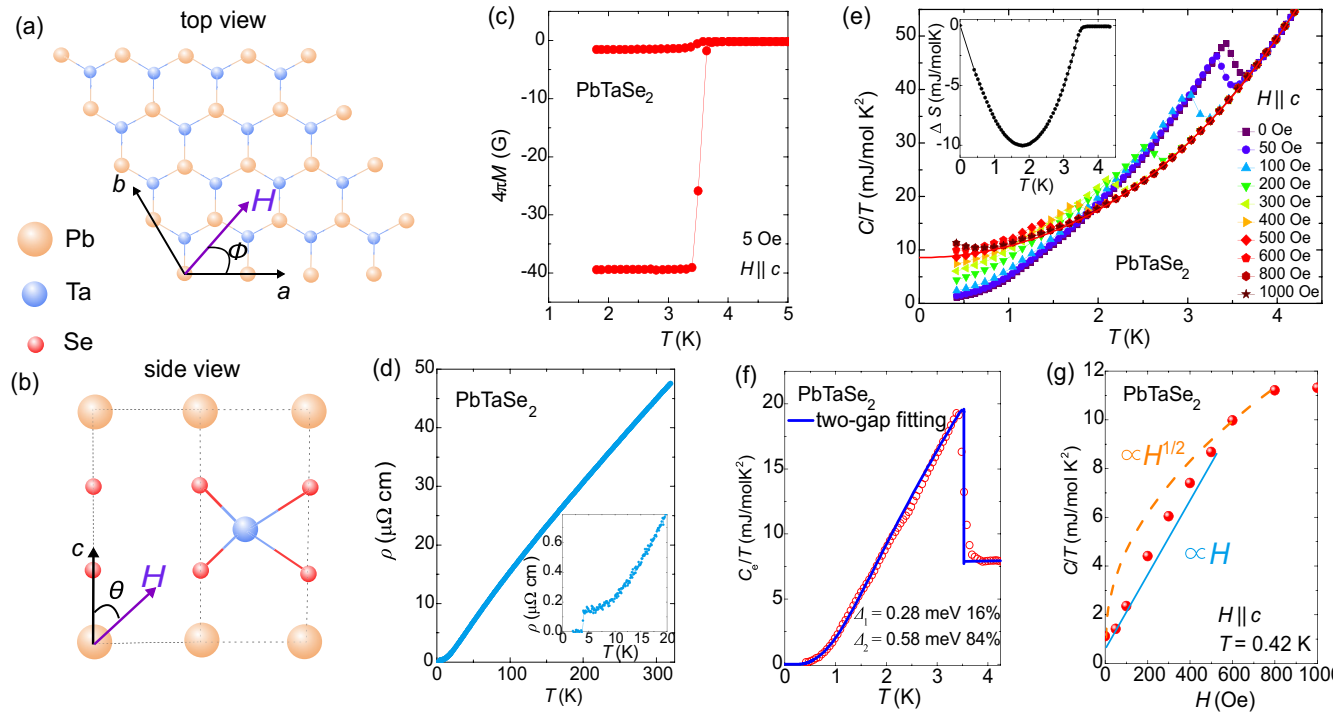

FIG. 1. Crystal structure of $PbTaSe_2$ in (a) the hexagonal plane from the top view, and (b) the noncentrosymmetric structure from the side view. The orange, blue, and red circles represent the elements of Pb, Ta, and Se, respectively. The definitions of the azimuthal angle ϕ and polar angle θ with respect to the crystal structure are also shown. (c) Temperature dependence of the magnetization under 5 Oe field perpendicular to the hexagonal plane. (d) Temperature dependence of the in-plane resistivity measured at zero field. The inset is the enlarged plot below 20 K. (e) Temperature dependence of specific heat plotted as C/T vs T under magnetic fields ($H \parallel c$) ranging from 0 to 1000 Oe. The solid line represents the fit to the normal state specific heat. The inset shows the temperature dependence of the difference between the superconducting and normal state entropies, ΔS. (f) Zero-field electronic specific heat C_e/T vs T, together with the fit by a two isotropic s-wave gap model. (g) Magnetic field dependence of specific heat at 0.42 K for $H \parallel c$. The solid and dashed lines represent the H and $H^{1/2}$ dependences.

QPs, while the latter one is phase sensitive. The superconductivity of $PbTaSe_2$ is found to be fully gapped, consisting of two isotropic s-wave gaps with sign-preserved pairing.

II. EXPERIMENT

$PbTaSe_2$ single crystals were grown by the chemical vapor transport method [32]. Magnetization measurements were performed using a commercial superconducting quantum interference device (SQUID) magnetometer (MPMS-XL5, Quantum Design). The resistivity was measured by the four-probe method in a physical property measurement system (PPMS, Quantum Design). The temperature dependence of the specific heat under various magnetic fields was also measured by using PPMS. The 3D field-angle dependence of the specific heat was measured in an 8-T split-pair superconducting magnet with a ^{3}He refrigerator. The refrigerator can be continuously rotated by a motor on top of the dewar with an angular resolution of better than 0.01°. The calibration and validity of the measurement system can be seen in our previous paper [33]. Single crystals used for the irradiation experiments were cleaved to thin plates with thickness ~30 μm along the c axis, which is smaller than the projected range of 3-MeV H^+ for $PbTaSe_2$ of ~47 μm [34]. To avoid a possible sample-dependent influence, all the measurements were performed on one identical piece of crystal, which was divided into several pieces and irradiated by H^+ up to doses of 0 (pristine), 0.5×10^{16}, 1×10^{16}, 2×10^{16}, 4×10^{16}, and 8×10^{16}/cm^2, respectively. We estimated that 1×10^{16} dose H^+ irradiation is supposed to cause about 1 vacancy per 3200 Pb atoms assuming no overlap. More details about the irradiation experiments can be seen in our previous publications [35–38].

III. RESULTS AND DISCUSSION

$PbTaSe_2$ consists of the stacking of hexagonal $TaSe_2$ layers intercalated with Pb. Figure 1(a) shows the crystal structure looking down the hexagonal $TaSe_2$ plane. The intercalated Pb atoms sit above the Se atoms, and make the crystal structure noncentrosymmetric as shown in the side view [Fig. 1(b)] [15,16]. ϕ defines the azimuthal angle of the magnetic field rotates in the hexagonal plane [Fig. 1(a)], while θ defines the polar angle of the magnetic field away from the c axis [Fig. 1(b)].

Figure 1(c) shows the temperature dependence of magnetic susceptibility, which displays $T_c \sim 3.7$ K (T_c is defined by the onset of the deviation between the zero-field-cooling and field-cooling susceptibilities) with a sharp transition width of less than 0.2 K by taking the criteria of 10% and 90% of the magnetization result at 1.8 K. The T_c is also confirmed

by the zero resistivity [see the inset of Fig. 1(d)]. The main panel of Fig. 1(d) shows the temperature dependence of the in-plane resistivity at a temperature range from 320 to 2 K. The residual resistivity ratio RRR defined as $\rho(300\ \mathrm{K})/\rho(T_c^{\mathrm{onset}})$ is estimated to be as large as ∼321. The sharp SC transition width and the large RRR confirm the high quality of the single crystal.

Figure 1(e) shows the temperature dependence of specific heat divided by temperature C/T under various magnetic fields ($H \parallel c$) ranging from 0 to 1000 Oe. A clear jump associated with the superconducting transition is observed at around 3.7 K under zero field, which is consistent with the susceptibility and resistivity measurements. The SC jump is gradually suppressed by magnetic field, and no SC jump can be observed down to ∼0.4 K under $H = 800$ Oe. On the other hand, an upturn can be observed at temperatures below ∼0.7 K when $H > 600$ Oe. The NMR measurements have proved that the electron-electron interaction is very weak in this material based on the observation that the spin-lattice relaxation rate varies in proportion to the temperature [26]. Therefore, such upturn behavior may be from the Schottky behavior of the nuclear contribution.

The normal state specific heat can be fitted by the sum of the electronic part and phononic part: $C_n/T = \gamma_n + \beta_n T^2 + \alpha_n T^4$. The fitting result is shown as the solid line in Fig. 1(e) giving $\gamma_n = 8.56\ \mathrm{mJ/mol\,K^2}$, $\beta_n = 2.12\ \mathrm{mJ/mol\,K^4}$, and $\alpha_n = 0.028\ \mathrm{mJ/mol\,K^6}$. The validity of the fitting is justified by the entropy conservation as shown in the inset of Fig. 1(e). In addition, a very small residual specific heat γ_0 under zero field at 0 K is obtained as $\sim 0.5\ \mathrm{mJ/mol\,K^2}$ by linearly extrapolating the data of C/T vs T^2 down to 0 K (see Supplemental Fig. S1 [39]). The normalized specific heat jump at T_c, $\Delta C/(\gamma_n - \gamma_0)T_c$, is estimated to be 1.39, which is close to the weak-coupling value 1.43 of BCS theory. A similar value of the normalized specific heat jump is also reported in a previous paper [15], while a slightly larger value ∼1.71 is also reported [23]. Zero-field electronic specific heat C_e/T obtained from subtracting the phonon terms is shown in Fig. 1(f). C_e/T decreases to a small value close to zero at low T, indicating the nodeless gap structure similar to previous reports [23,24]. On the other hand, C_e/T increases linearly with T in a wide temperature region above $T = 1$ K, which is different from the exponential increase for a single-gapped isotropic s-wave superconductor. The fitting of C_e will be discussed later.

More information about the gap structure can be obtained from the magnetic field dependence of the specific heat, C/T vs H, which usually reflects the QPs' excitation within the SC gap. For a superconductor with an isotropic single gap, $C(H)/T$ is linearly related to H [$C(H) \sim C_n(H/0.8H_{c2})$ under small field, where C_n is the normal state specific heat, and H_{c2} is the upper critical field] because the low-energy QPs are mainly localized in the vortex core, whose density is proportional to H [40]. For a single gap with nodes, $C(H)/T$ is not linearly proportional to H ($\propto H^{1/2}$ for the line nodes, and $\propto H^{0.64}$ for the point nodes [41]) because of the QPs' Doppler shift caused by supercurrents around the vortex core [42]. In between, $C(H)/T$ for an anisotropic single gap or multigaps shows a crossover from linear-H to $H^{1/2}$ dependence [40]. The $C(H)/T$ of $PbTaSe_2$ at 0.42 K for $H \parallel c$ is shown in Fig. 1(g), which resides between the linear and $H^{1/2}$ behaviors. This result excludes the single isotropic gap structure, the line or loop nodes (both vertical or horizontal), and the point nodes in the ab plane. However, the point nodes along the c axis cannot be excluded by the measurements with $H \parallel c$ because the low-energy QPs will not be excited when the field is parallel to the nodal direction. Besides, the anisotropic single gap and multigaps cannot be distinguished in the $C(H)/T$ results.

Therefore, only the temperature and field-dependent specific heat results cannot reveal the angle-resolved gap structure of $PbTaSe_2$. According to the Doppler shift effect, $\delta E = m_e \boldsymbol{v}_F \cdot \boldsymbol{v}_s$ (m_e is the electron mass, $\mathbf{v}_F$ is the Fermi velocity, and $\mathbf{v}_s$ is the local superfluid velocity always perpendicular to the field) [42], the zero-energy density of states (DOS) under small fields in superconductors with nodes or gap minima depends on the direction of the field with respect to the nodal/gap minimum positions. When $H \parallel$ nodes/gap minima, it shows minima because $\delta E = 0$ in the case of $\mathbf{v}_F \perp \mathbf{v}_s$, while it turns into maxima when $H \perp$ nodes/gap minima because δE becomes maximal in the situation of $\mathbf{v}_F \parallel \mathbf{v}_s$. Therefore, in the low-field region, specific heat shows minima for $H \parallel$ node/gap minimum, and maxima for $H \perp$ node/gap minimum. On the other hand, under high fields, the QP scattering by the magnetic field is strongly enhanced, exciting a much higher finite-energy DOS around the nodal positions for $H \parallel$ node/gap minimum. When the finite-energy DOS overcomes the zero-energy DOS, the oscillation switches signs, i.e., specific heat becomes maxima for $H \parallel$ node/gap minimum, but minima for $H \perp$ node/gap minimum [43,44]. Such sign change behavior has been observed in superconductors with nodes [45,46] or gap minima [47,48]. By contrast, for the isotropic gap structure, the specific heat should be independent of the field direction. To reveal the angle-resolved gap structure of $PbTaSe_2$, we turn to the measurements of specific heat under magnetic field with angle resolution.

Figures 2(a)– 2(d) show the azimuthal angle-resolved specific heat $\Delta C(\phi)/T$ under different magnetic fields at 0.35, 1, 2.1, and 3.2 K, respectively. Obviously, no oscillation is observed at any temperature and field. Usually the magnitude of the oscillation from nodes/gap minima is about a few percent of the total electronic specific heat $C_e(H)$ [47,49]. In Supplemental Fig. S2, we show that the noise level of our system is $\sim 0.07\ \mathrm{mJ/mol\,K^2}$ at 0.35 K and 0.08 T. In this case, an oscillatory signal (e.g., twofold anisotropy) in the $\Delta C(\phi)/T$ with an amplitude of 1%–3% of C_e/T should still be observed if it exists (see Supplemental Material S2 [39]). Therefore, our azimuthal angle-resolved specific heat results confirm that the in-plane gap structure should be nearly isotropic, although we cannot exclude the possibility of very tiny anisotropy below our resolution limit. On the other hand, the out-of-plane gap structure cannot been resolved only by the azimuthal angle-resolved measurements, because the point nodes/gap minima along the c axis will not cause oscillation in $\Delta C(\phi)/T$ [46,50].

In order to probe the gap structure along the c axis, and reveal the 3D gap structure of $PbTaSe_2$, we also measured the polar-angle dependence of the specific heat $\Delta C(\theta)/T$ (see Fig. 3). If the point nodes/gap minima along the c axis are present, the $\Delta C(\theta)/T$ is expected to show an oscillatory

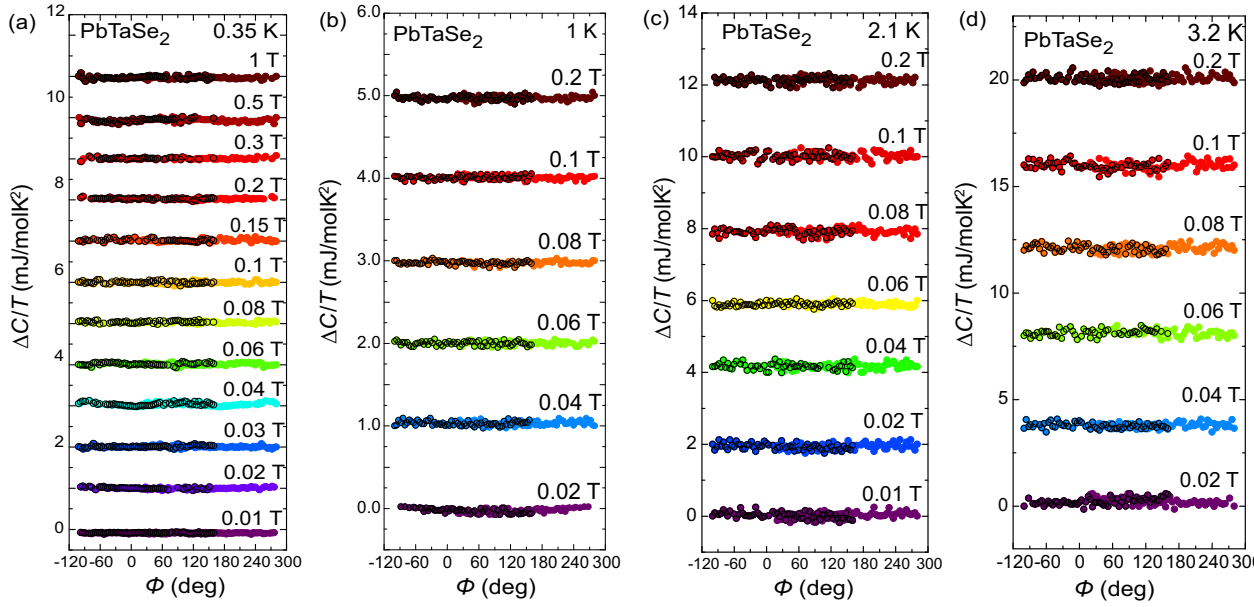

FIG. 2. Azimuthal angle dependence of the specific heat $\Delta C(\phi)/T$ measured under various fields at (a) 0.35 K, (b) 1 K, (c) 2.1 K, and (d) 3.2 K, respectively. Each subsequent curve at the same temperature is shifted vertically to show the angle dependence more clearly. Black-outlined symbols are the measured data; the others are mirrored points to show the angle dependence more clearly.

behavior with a sign change as discussed above. Nevertheless, $\Delta C(\theta)/T$ does not display such features. Instead, it manifests a twofold symmetry at low temperature such as 0.35 K under small fields [see Fig. 3(a)], which is simply attributed to the out-of-plane anisotropy of H_{c2}. Under larger fields, $\Delta C(\theta)/T$ becomes flat (θ independent) at the θ range around 0, which comes from the suppression of SC for $H \parallel c$ ($\theta = 0$) due to the small H_{c2}. Subsequently, the flattened region evolves into a wider θ range with further increasing field. Finally, the $\Delta C(\theta)/T$ becomes totally θ independent at 0.3 T, indicating that the H_{c2} is reached also for $H \parallel ab$ ($\theta = \pm 90^\circ$). The out-of-plane anisotropy is consistent with that obtained from transport and magnetic susceptibility measurements [23,32].

On the other hand, at higher temperatures, $\Delta C(\theta)/T$ shows some special features such as the peaks when $H \parallel ab$ ($\theta = \pm 90^\circ$) at 2.1 K for $H \geqslant 0.04$ T [see Fig. 3(c)]. These features

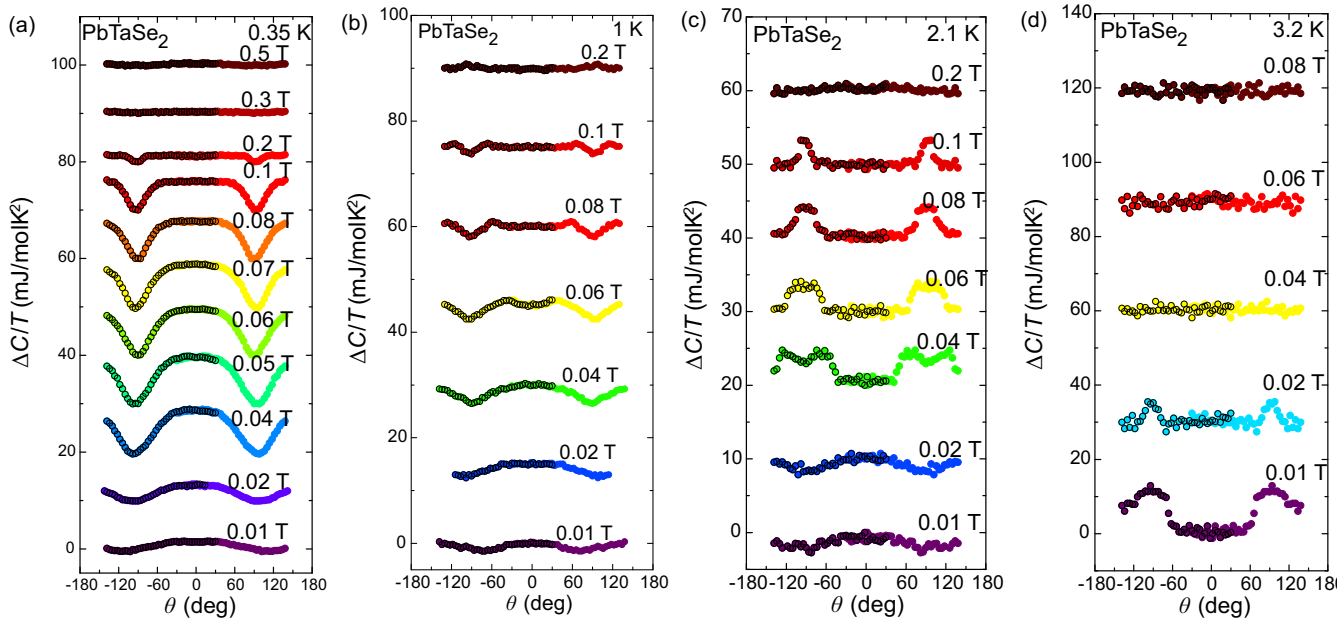

FIG. 3. Polar angle dependence of the specific heat $\Delta C(\theta)/T$ measured under various fields at (a) 0.35 K, (b) 1 K, (c) 2.1 K, and (d) 3.2 K, respectively. Each subsequent curve at the same temperature is shifted vertically to show the angle dependence more clearly. Black-outlined symbols are the measured data; the others are mirrored points to show the angle dependence more clearly.

are different from the sign change behavior induced by the nodal gap structure. In the θ range around 0°, $\Delta C(\theta)/T$ at 2.1 K already becomes θ independent for $H \geqslant 0.04$ T, which suggests that it is in the normal state. Meanwhile, $\Delta C(\theta)/T$ around ±90° stays in the SC state. The larger $\Delta C(\theta = \pm 90°)/T$ than $\Delta C(\theta = 0°)/T$ originates from the larger specific heat in the SC state close to T_c than that in the normal state. The dips at $\theta = \pm 90°$ observed at 2.1 K and 0.04 T are due to the crossover from the minimum to peak.

Here, we emphasize that the relatively large out-of-plane anisotropy induces a strong oscillation in $\Delta C(\theta)/T$, which may cover the feature from possible c-axis nodes such as the sign change behavior. Therefore, we cannot simply exclude the c-axis point nodes only by the $\Delta C(\theta)/T$ results. To have more evidence, we also measured the $C(H)/T$ with $H \parallel ab$ at 0.33 K as shown in Fig. S3 [39]. The field dependence of $C(H)/T$ obviously deviates from the expected behavior of $\propto H^{0.64}$ for the point nodes [41]. It increases linearly with magnetic field with different slopes in the low-field and high-field regions, representing the behavior of a two-gap superconductor. Those results confirm that there are no c-axis point nodes in $PbTaSe_2$.

Now, we return to the temperature dependence of C_e/T shown in Fig. 1(f). Based on the above discussions, we fit the C_e/T with a two-gap model based on the BCS theory by simply assuming Δ_1 and Δ_2 are both isotropic s waves. In this case, $C_e = \eta_1 C_2(\Delta_1) + \eta_2 C_2(\Delta_2)$, where C_i denotes the electronic specific heat for each gap, while η_i denotes the ratio of each gap. The data are well fitted, as shown by the solid line in Fig. 1(f), with the gap values $\Delta_1 = 0.28$ meV and $\Delta_2 = 0.58$ meV, and a relative weight of $\eta_1 = 16\%$, and $\eta_2 = 84\%$. A two-gap model with two isotropic s-wave gaps has been also applied in the fitting of the conductance curve of STM [14].

Until now, the temperature, field, and angle dependences of specific heat have confirmed that the bulk gap structure of $PbTaSe_2$ consists of two 3D isotropic s waves. However, even for the s-wave gap structure, the gap function can be sign reversed or preserved. The sign-reversed s wave, usually called $s_\pm$, has been suggested to be the most plausible gap function of iron-based superconductors [30,31]. The amount of excited QPs should be the same for both the sign-reversed and sign-preserved s wave. Therefore, to distinguish the two possible gap functions, a phase-sensitive technique is needed. The nonmagnetic disorder effect induced by light-particle irradiation, such as the electron and H^+, has been proven to be an effective method to discriminate the sign-reversed s wave from the sign-preserved one. For the sign-reversed $s_\pm$, T_c is usually suppressed remarkably by the nonmagnetic disorders, while T_c for the sign-preserved s wave is robust [52,55].

The H^+-irradiation effect on $PbTaSe_2$ is summarized and presented in Fig. 4. It should be noted that $PbTaSe_2$ contains the topological surface state, whose gap function is reported to be different from the bulk one, which may have nodes [56,57]. To avoid the possible influence of the surface state, T_c's for the H^+-irradiated crystals were probed by both magnetic susceptibility and resistivity measurements as shown in Figs. 4(a) and 4(b), respectively. Obviously, the irradiated crystals display

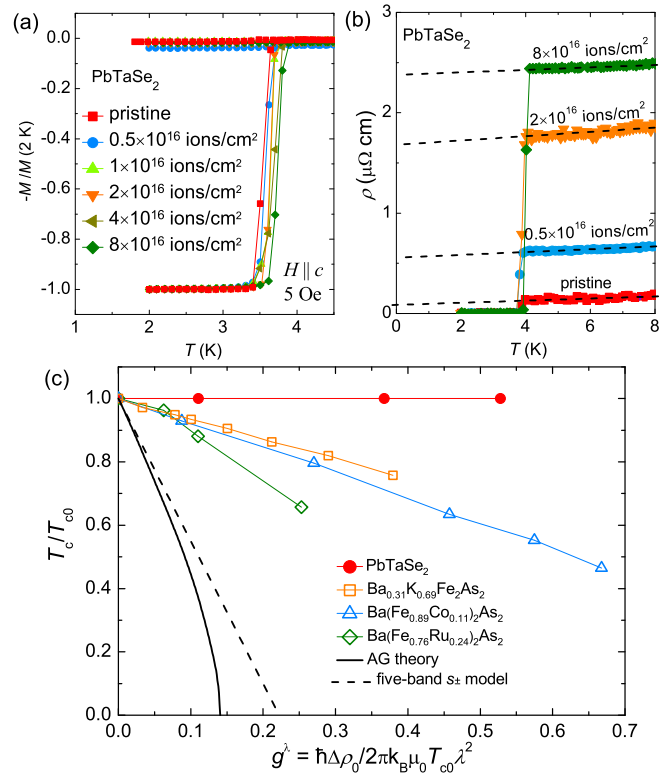

FIG. 4. (a) Temperature dependence of the normalized magnetization at 5 Oe for pristine and H^+-irradiated crystals. (b) Temperature dependence of the resistivity for the pristine and some selected irradiated crystals. Dashed lines are the linear extrapolations to zero temperature for estimating the residual resistivity ρ_0. (c) T_c/T_{c0} as a function of a dimensionless scattering rate $g^\lambda = \hbar\Delta\rho_0/2\pi k_B \mu_0 T_{c0}\lambda^2$. The solid line is the T_c suppression rate predicted by the Abrikosov-Gor'kov (AG) theory for an isotropic s-wave superconductor with magnetic impurities [51]. The dashed line represents the theoretical prediction by a five-band $s_\pm$ model [52]. For comparison, we also plot the results from the $Ba_{0.31}K_{0.69}Fe_2As_2$ [35], $Ba(Fe_{0.89}Co_{0.11})_2As_2$ [53], and $Ba(Fe_{0.76}Ru_{0.24})_2As_2$ [54] with possible $s_\pm$ pairing.

nearly the same T_c as the pristine one, which proves that there is no node in the gap structure, otherwise T_c will be suppressed with smearing the nodes by introducing disorders. This result is consistent with the observation from specific heat.

For a quantitative discussion of the pairing-breaking effect and a comparison with other superconductors, the T_c suppression rate T_c/T_{c0} is plotted against the dimensionless scattering rate g^λ as shown in Fig. 4(c), where T_c is obtained from the resistivity measurements shown in Fig. 4(b), and T_{c0} is the value of T_c for the pristine one. $g^\lambda = \hbar\Delta\rho_0/2\pi k_B \mu_0 T_{c0}\lambda^2$ [58], where $\hbar$ is the Planck's constant divided by 2π, k_B is the Boltzmann constant, μ_0 is the vacuum permeability, and λ is the penetration depth $\backsimeq$204 nm evaluated from a tunnel diode oscillator experiment [25]. $\Delta\rho_0$ is the increase of residual resistivity after irradiation, $\Delta\rho_0 = \rho_0^{\text{irradiated}} - \rho_0^{\text{pristine}}$. The residual resistivity ρ_0 was obtained by linearly extrapolating ρ-T curves in the normal state above T_c to $T = 0$ K, as shown by the dashed lines in Fig. 4(b). In the plot of T_c/T_{c0} vs g^λ, the disorder level is expressed by the ρ_0, evaluated simultaneously with T_c in the ρ-T measurements, which avoids the influence

from possible thermal annealing after irradiation. Indeed, the increase of ρ_0 for the crystal irradiated by $8 \times 10^{16}/\mathrm{cm}^2$ of H^+ is smaller than expected, indicating the possible annealing effect before measurements after irradiation.

For comparison, we also plot the T_c suppression rates expected by the Abrikosov-Gor'kov (AG) theory for an isotropic *s*-wave superconductor with magnetic impurities (solid line) [51], and that by a five-band $s_\pm$ model (dashed line) [52], together with those from $Ba_{0.31}K_{0.69}Fe_2As_2$ [35], $Ba(Fe_{0.89}Co_{0.11})_2As_2$ [53], and $Ba(Fe_{0.76}Ru_{0.24})_2As_2$ [54] with possible $s_\pm$ pairing. Clearly, the T_c suppression rate for $PbTaSe_2$ is much smaller than those theories and materials. Recently, sign-preserved pairing was discussed on the heavy-fermion $CeCu_2Si_2$ based on the observation of robust superconductivity against impurities [59]. On the other hand, similar behavior of an unchanged T_c against H^+ and electron irradiation has been observed in an established two-gap s_{++} superconductor MgB_2 [60,61]. Therefore, such robust T_c to the disorders demonstrates that the gap function of $PbTaSe_2$ should be sign preserved rather than sign reversed. Thus, our combined ARSH and disorder effect studies have proved that $PbTaSe_2$ consists of two isotropic *s*-wave gaps without a sign reversal.

IV. CONCLUSIONS

In summary, we have investigated the bulk superconducting gap function of the topological superconductor $PbTaSe_2$ through the combined studies of ARSH and the disorder effect. Temperature, magnetic field, and 3D angle dependences of specific-heat measurements prove that the superconductivity of $PbTaSe_2$ is fully gapped, with two isotropic *s*-wave gaps. The superconducting transition temperature T_c is found to be robust against nonmagnetic disorders induced by H^+ irradiation, which suggests that the gap functions should have the same sign.

ACKNOWLEDGMENTS

This work was partly supported by JSPS KAKENHI (Grants No. JP20H05164, No. JP19K14661, No. 18H05853, No. 18H01161, No. 18H04306, No. 17K05553, No. 17H01141, and No. 15H05883), and the National Natural Science Foundation of China (Grants No. U1932217, No. 11674054, and No. U1732162). R.S. acknowledges financial support provided by the Ministry of Science and Technology in Taiwan under Grant No. MOST-108-2112-M-001-049-MY2.

[1] X.-L. Qi and S.-C. Zhang, Rev. Mod. Phys. **83**, 1057 (2011).
[2] M. Sato and Y. Ando, Rep. Prog. Phys. **80**, 076501 (2017).
[3] A. Kitaev, Ann. Phys. **303**, 2 (2003).
[4] C. Nayak, S. H. Simon, A. Stern, M. Freedman, and S. Das Sarma, Rev. Mod. Phys. **80**, 1083 (2008).
[5] L. Fu and C. L. Kane, Phys. Rev. Lett. **100**, 096407 (2008).
[6] X.-L. Qi, T. L. Hughes, and S.-C. Zhang, Phys. Rev. B **82**, 184516 (2010).
[7] S. Nadj-Perge, I. K. Drozdov, B. A. Bernevig, and A. Yazdani, Phys. Rev. B **88**, 020407(R) (2013).
[8] C. Beenakker, Annu. Rev. Condens. Matter Phys. **4**, 113 (2013).
[9] S. Sasaki, M. Kriener, K. Segawa, K. Yada, Y. Tanaka, M. Sato, and Y. Ando, Phys. Rev. Lett. **107**, 217001 (2011).
[10] L. Fu and E. Berg, Phys. Rev. Lett. **105**, 097001 (2010).
[11] P. Zhang, Z. Wang, X. Wu, K. Yaji, Y. Ishida, Y. Kohama, G. Dai, Y. Sun, C. Bareille, K. Kuroda, T. Kondo, K. Okazaki, K. Kindo, X. Wang, C. Jin, J. Hu, R. Thomale, K. Sumida, S. Wu, K. Miyamoto *et al.*, Nat. Phys. **15**, 41 (2019).
[12] M. Sato and S. Fujimoto, Phys. Rev. B **79**, 094504 (2009).
[13] S. Yip, Annu. Rev. Condens. Matter Phys. **5**, 15 (2014).
[14] S.-Y. Guan, P.-J. Chen, M.-W. Chu, R. Sankar, F. Chou, H.-T. Jeng, C.-S. Chang, and T.-M. Chuang, Sci. Adv. **2**, e1600894 (2016).
[15] M. N. Ali, Q. D. Gibson, T. Klimczuk, and R. J. Cava, Phys. Rev. B **89**, 020505(R) (2014).
[16] G. Bian, T.-R. Chang, R. Sankar, S.-Y. Xu, H. Zheng, T. Neupert, C.-K. Chiu, S.-M. Huang, G. Chang, I. Belopolski, D. S. Sanchez, M. Neupane, N. Alidoust, C. Liu, B. Wang, C.-C. Lee, H.-T. Jeng, C. Zhang, Z. Yuan, S. Jia *et al.*, Nat. Commun. **7**, 10556 (2016).
[17] S. S. Zhang, J.-X. Yin, G. Dai, L. Zhao, T.-R. Chang, N. Shumiya, K. Jiang, H. Zheng, G. Bian, D. Multer, M. Litskevich, G. Chang, I. Belopolski, T. A. Cochran, X. Wu, D. Wu, J. Luo, G. Chen, H. Lin, F.-C. Chou, X. Wang, C. Jin, R. Sankar, Z. Wang, and M. Z. Hasan, Phys. Rev. B **101**, 100507(R) (2020).
[18] T.-R. Chang, P.-J. Chen, G. Bian, S.-M. Huang, H. Zheng, T. Neupert, R. Sankar, S.-Y. Xu, I. Belopolski, G. Chang, B. K. Wang, F. Chou, A. Bansil, H.-T. Jeng, H. Lin, and M. Z. Hasan, Phys. Rev. B **93**, 245130 (2016).
[19] C. Q. Xu, R. Sankar, W. Zhou, B. Li, Z. D. Han, B. Qian, J. H. Dai, H. Cui, A. F. Bangura, F. C. Chou, and X. Xu, Phys. Rev. B **96**, 064528 (2017).
[20] X. Xu, Z. Kang, T.-R. Chang, H. Lin, G. Bian, Z. Yuan, Z. Qu, J. Zhang, and S. Jia, Phys. Rev. B **99**, 104516 (2019).
[21] C.-S. Lian, C. Si, and W. Duan, Phys. Rev. B **100**, 235420 (2019).
[22] M. N. Wilson, A. M. Hallas, Y. Cai, S. Guo, Z. Gong, R. Sankar, F. C. Chou, Y. J. Uemura, and G. M. Luke, Phys. Rev. B **95**, 224506 (2017).
[23] C.-L. Zhang, Z. Yuan, G. Bian, S.-Y. Xu, X. Zhang, M. Z. Hasan, and S. Jia, Phys. Rev. B **93**, 054520 (2016).
[24] M. X. Wang, Y. Xu, L. P. He, J. Zhang, X. C. Hong, P. L. Cai, Z. B. Wang, J. K. Dong, and S. Y. Li, Phys. Rev. B **93**, 020503(R) (2016).
[25] G. M. Pang, M. Smidman, L. X. Zhao, Y. F. Wang, Z. F. Weng, L. Q. Che, Y. Chen, X. Lu, G. F. Chen, and H. Q. Yuan, Phys. Rev. B **93**, 060506(R) (2016).
[26] S. Maeda, K. Matano, and G.-q. Zheng, Phys. Rev. B **97**, 184510 (2018).
[27] S. Kobayashi and M. Sato, Phys. Rev. Lett. **115**, 187001 (2015).
[28] T. Hashimoto, S. Kobayashi, Y. Tanaka, and M. Sato, Phys. Rev. B **94**, 014510 (2016).
[29] S. A. Yang, H. Pan, and F. Zhang, Phys. Rev. Lett. **113**, 046401 (2014).
[30] I. I. Mazin, Nature (London) **464**, 183 (2010).
[31] P. J. Hirschfeld, M. M. Korshunov, and I. I. Mazin, Rep. Prog. Phys. **74**, 124508 (2011).

[32] S. Raman, G. N. Rao, I. P. Muthuselvam, C. Tay-Rong, H. T. Jeng, G. S. Murugan, L. Wei-Li, and F. C. Chou, J. Phys.: Condens. Matter **29**, 095601 (2017).
[33] Y. Sun, S. Kittaka, T. Sakakibara, K. Machida, J. Wang, J. Wen, X. Xing, Z. Shi, and T. Tamegai, Phys. Rev. Lett. **123**, 027002 (2019).
[34] J. Ziegler, J. Biersack, and U. Littmark, *The Stopping and Range of Ions in Solids* (Pergamon, New York, 1985).
[35] T. Taen, F. Ohtake, H. Akiyama, H. Inoue, Y. Sun, S. Pyon, T. Tamegai, and H. Kitamura, Phys. Rev. B **88**, 224514 (2013).
[36] Y. Sun, A. Park, S. Pyon, T. Tamegai, and H. Kitamura, Phys. Rev. B **96**, 140505(R) (2017).
[37] A. Park, S. Pyon, Y. Sun, I. Veshchunov, J. Chen, N. Ito, T. Suwa, T. Tamegai, H. Kitamura, and A. Ichinose, Phys. Rev. B **98**, 054512 (2018).
[38] Y. Sun, S. Pyon, T. Tamegai, R. Kobayashi, T. Watashige, S. Kasahara, Y. Matsuda, T. Shibauchi, and H. Kitamura, Appl. Phys. Express **8**, 113102 (2015).
[39] See Supplemental Material at http://link.aps.org/supplemental/10.1103/PhysRevB.102.024517 for the estimation of the residual specific heat, the noise level of the azimuthal angle dependence of specific heat, and the magnetic field dependence of specific heat at 0.33 K for $H \parallel ab$.
[40] N. Nakai, P. Miranović, M. Ichioka, and K. Machida, Phys. Rev. B **70**, 100503(R) (2004).
[41] P. Miranović, N. Nakai, M. Ichioka, and K. Machida, Phys. Rev. B **68**, 052501 (2003).
[42] G. E. Volovik, JETP Lett. **58**, 469 (1993).
[43] A. Vorontsov and I. Vekhter, Phys. Rev. Lett. **96**, 237001 (2006).
[44] M. Hiragi, K. M. Suzuki, M. Ichioka, and K. Machida, J. Phys. Soc. Jpn. **79**, 094709 (2010).
[45] K. An, T. Sakakibara, R. Settai, Y. Onuki, M. Hiragi, M. Ichioka, and K. Machida, Phys. Rev. Lett. **104**, 037002 (2010).
[46] S. Kittaka, Y. Shimizu, T. Sakakibara, Y. Haga, E. Yamamoto, Y. Ōnuki, Y. Tsutsumi, T. Nomoto, H. Ikeda, and K. Machida, J. Phys. Soc. Jpn. **85**, 033704 (2016).
[47] Y. Sun, S. Kittaka, S. Nakamura, T. Sakakibara, K. Irie, T. Nomoto, K. Machida, J. Chen, and T. Tamegai, Phys. Rev. B **96**, 220505(R) (2017).
[48] Y. Sun, S. Kittaka, S. Nakamura, T. Sakakibara, P. Zhang, S. Shin, K. Irie, T. Nomoto, K. Machida, J. Chen, and T. Tamegai, Phys. Rev. B **98**, 064505 (2018).
[49] T. Sakakibara, S. Kittaka, and K. Machida, Rep. Prog. Phys. **79**, 094002 (2016).
[50] Y. Tsutsumi, T. Nomoto, H. Ikeda, and K. Machida, Phys. Rev. B **94**, 224503 (2016).
[51] A. A. Abrikosov and L. P. Gor'kov, Zh. Eksp. Teor. Fiz. **39**, 1781 (1960) [Sov. Phys. JETP 12, 1243 (1961)] .
[52] S. Onari and H. Kontani, Phys. Rev. Lett. **103**, 177001 (2009).
[53] Y. Nakajima, T. Taen, Y. Tsuchiya, T. Tamegai, H. Kitamura, and T. Murakami, Phys. Rev. B **82**, 220504(R) (2010).
[54] R. Prozorov, M. Kończykowski, M. A. Tanatar, A. Thaler, S. L. Bud'ko, P. C. Canfield, V. Mishra, and P. J. Hirschfeld, Phys. Rev. X **4**, 041032 (2014).
[55] Y. Wang, A. Kreisel, P. J. Hirschfeld, and V. Mishra, Phys. Rev. B **87**, 094504 (2013).
[56] T. Le, Y. Sun, H.-K. Jin, L. Che, L. Yin, J. Li, G. M. Pang, C. Q. Xu, L. X. Zhao, S. Kittaka, T. Sakakibara, K. Machida, R. Sankar, H. Q. Yuan, G. F. Chen, X. Xu, S. Li, Y. Zhou, and X. Lu, Sci. Bull. **65**, 1349 (2020).
[57] H.-K. Jin, D.-H. Xu, and Y. Zhou, arXiv:1905.11584.
[58] V. G. Kogan, Phys. Rev. B **80**, 214532 (2009).
[59] T. Yamashita, T. Takenaka, Y. Tokiwa, J. A. Wilcox, Y. Mizukami, D. Terazawa, Y. Kasahara, S. Kittaka, T. Sakakibara, M. Konczykowski, S. Seiro, H. S. Jeevan, C. Geibel, C. Putzke, T. Onishi, H. Ikeda, A. Carrington, T. Shibauchi, and Y. Matsuda, Sci. Adv. **3**, e1601667 (2017).
[60] T. Klein, R. Marlaud, C. Marcenat, H. Cercellier, M. Konczykowski, C. J. van der Beek, V. Mosser, H. S. Lee, and S. I. Lee, Phys. Rev. Lett. **105**, 047001 (2010).
[61] E. Mezzetti, D. Botta, R. Cherubini, A. Chiodoni, R. Gerbaldo, G. Ghigo, G. Giunchi, L. Gozzelino, and B. Minetti, Physica C **372**, 1277 (2002).